Effect of Angle of Attack on Vibration Characteristics of a Cantilevered Prism for Energy Harvest

Takahiro Kiwata[+1], Aguri Nakajima[+2], Shunichi Mizukami[+3], Toshiyuki Ueno[+4] and Takaaki Kono[+5]

[+1] Research Center for Sustainable Energy and Technology, Kanazawa University, Kakuma-machi, Kanazawa-shi, Ishikawa, 920-1192, Japan
[+2] Graduate School of Natural Science and Technology, Kanazawa University
[+3] Graduate School of Natural Science and Technology, Kanazawa University
[+4] School of Electrical and Computer Engineering, Kanazawa University
[+5] Research Center for Sustainable Energy and Technology, Kanazawa University

To develop the power generation system using iron-gallium alloy, we focus on the transverse galloping vibration for a rectangular prism with a critical depth section of less than the side ratio $D/H \approx 0.6$, and for a D-section prism which vibrates at a reduced velocity V_r ($=U/f_cH$) lower than the resonant velocity. The free vibration test using a plate spring was carried out in the water tunnel to investigate effects of the angle of attack and the vibration direction on the vibration characteristics. The vibration direction I of the prism is the same as the longitudinal direction of the prism. The vibration direction II of the prism is the same as the transverse direction to flow. We also carried out a power generation experiment using the iron-gallium alloy to investigate effects of angle of attack on energy harvesting. The D-section prism with the side ratio of 0.23 for the vibration direction I vibrates at a wide range of angle of attack in comparison with the other prisms. The maximum electric power P using a D-section prism with D/H=0.23 is 26 mW at $V_r = 4.15$.

Keyword: Flow-Induced Vibration, Low-Speed Galloping, Rectangular Prism, Angle of Attack, Energy Harvesting

1. INTRODUCTION

The carbon dioxide emissions that lead to global warming are increased by the fossil fuel consumption in the world. To present of global warming, countries are proceeding the development of technologies for utilizing renewable power sources, i.e. solar, wind, biomass and hydraulic powers, in recent years. Although the utilization of vibrations for power generation is not new technology, a number of researches have recently investigated the harvesting of power from various vibrations[1)]. Therefore, a large variety types of power generators that use flow-induced vibration has been invented, e.g., power generation of the vortex-induced vibration using tandem circular cylinders having electrical coils with steel cores and a ferrite magnet[2)], hydroelectric power generation using an inverted pendulum formed by a cylindrical body[3)], wave energy power generation using a piezoelectric element[4)], power generation by mechanical vibration due to the fluid-structure interaction between a flexible belt and the airflow[5)], wind energy harvester of a T-shaped piezoelectric bimorph cantilever[6)], electromagnetic generator using the galloping vibration of a lightweight box having a square, triangular, or semicircular cross-section[7)], and piezoelectric energy harvester using flapping-foils flutter vibration occur[8)]. However, these devices have not seem to be able to provide sufficient electric energy. Practical applications require a mechanism that will generate vibration in the presence of a low-velocity flow. In order to harvest energy from flowing water, we need to develop a simple and efficient power generator using a structure that flow-induced vibration occurs.

The relationship between galloping vibration and geometry of a structure has investigated by a number of researchers[9)-22)] for more than half a century. Galloping vibration is characterized by large amplitude

[+1]kiwata@se.kanazawa-u.ac.jp, [+2]anakajima@ryuko.ms.t.kanazawa-u.ac.jp, [+3]mizukami@ryuko.ms.t.kanazawa-u.ac.jp, [+4]ueno@ec.t.kanazawa-u.ac.jp, [+5]t-kono@se.kanazawa-u.ac.jp

vibrations normal to the direction of flow, which causes damage to the structures in some cases. Although most of the effort in galloping vibration research has been concentrated in bodies with square or rectangular cross-sections[9)-13)], the galloping-induced vibrations primarily occur in flexible and lightly damped structures with special and non-axisymmetric cross-sections such as D-shaped, L-shaped, cross-shaped, triangular and trapezium prisms[16)-22)].

To develop the power generation system using iron-gallium alloy[23)], we focus on transverse galloping for a rectangular prism with a critical depth section of less than $D/H \approx 0.6$ (where D: depth of a prism in the flow direction, H: height of a prism normal to the flow direction), and a D-section (semi-circle) prism, which vibrate at a flow velocity lower than the resonant velocity[12)-15)]. For the low-speed galloping, the transverse vibration depends on lateral force coefficient C_{FY} which varies as angle of attacks varies so that many researcher investigate influence of angle of attack on aerodynamics forces, i.e., drag and lift coefficients for various shape of cross-sections[11),17),18),29)-32)]. However, there are a little study about the effect of angle of attack on vibration characteristics[32),33)]. The purpose of the present study is to investigate the effect of angle of attack on the transverse galloping vibration of cantilevered rectangular and D-section prisms, and the performance of a power generator using an iron-gallium alloy as a magnetostrictive material and cantilevered prisms in a water tunnel.

2. EXPERIMENTAL APPARATUS AND METHOD

(1) Water tunnel

A schematic diagram of the experimental apparatus is shown in Figure 2. The experiments were performed in a water tunnel with a rectangular working section having a height of 400 mm, a width of 167 mm, and a length of 780 mm. A variable-frequency induction motor and an inverter (YASUKAWA ELECTRIC, VRISPEED-686SS5) were used to drive a double suction centrifugal pump (DMW, DF-SC). In the experiment, the water velocity U was changed from 1.0 m/s to 2.7 m/s by controlling the pump rotational speed. The Reynolds number Re (= UH/ν; ν, kinematic viscosity of water) was in the range of 2×10^4 to 5×10^4. The non-uniform level and the turbulence intensity in the working section at a water speed of $U = 1.5$ m/s were less than ±1.5% and about 2.0%, respectively.

(2) Test models and experimental method for free vibration

The experiment used rectangular and D-section prisms constructed of stainless steel with a smooth surface and sharp edges, as shown in Figure 3. Table 1(a) shows the specifications of the test prisms. Table 2(a) also shows the natural frequency of the test prisms. All prisms had a cross-section height H of 20 mm. The side ratio D/H of the rectangular prism was varied 0.2 and 0.5. The side ratio D/H of the D-section prism was varied 0.23 and 0.5. The span length of prisms L was 200 mm, and the aspect ratio was 10. The prism was mounted elastically to a plate spring attached to the ceiling wall of the test section with a jig as shown in Figure 2(a). The jig can change an angle of attack α of the prism between 5° and 60°. Furthermore, we investigated the effect of the vibration direction of the prism, namely, the vibration direction I of the prism is the same as the longitudinal direction of the prism, and the vibration direction II of the prism is the same as the transverse direction to flow. The characteristic frequency f_c of the prism was adjusted to a constant value between 22 and 46 Hz by using different plate springs. The tip displacement of the prism y and the characteristic frequency of the tested model f_c were measured using an acceleration sensor (Showa measuring instruments, 2302CW) implanted inside the tip of the prism using an integrator and an FFT analyzer (Ono sokki, CF-5201). The output signals of the integrator were converted using a 12-bit A/D converter with a sampling frequency of 2 kHz, and 10^4 data points were stored. The root-mean-square value of the fluctuation of displacement of a prism tip y_{rms}, reduced velocity V_r (= U/f_cH) or $\overline{V}_r$ (= $Uf_c/\overline{H}$) and non-dimensional amplitudes η_{rms} (= y_{rms}/H) or $\overline{\eta}_{rms}$ (= $y_{rms}/\overline{H}$) was calculated using a personal computer.

(3) Test models and experimental method for vibration-power generation

Figure 2(b) shows the experimental setup in the water tunnel in order to investigate the performance of the vibration-power generation device. Tables 1(b) and 2(b) show the specifications and natural frequency of the test models. The rectangular prisms had a cross-section height H of 20 mm and a span length L of 350 mm. We use the two test models that have different cross-section rectangular prism with $D/H = 0.2$ and D-section

prism with D/H = 0.23. The power-generation device was placed in an airtight acrylic resin box in order to prevent water intrusion. The Galfenol beam acted as a plate spring. The Galfenol had a tensile strength of 200 MPa. The dimensions of Galfenol beams were 5 mm × 3 mm × 100 mm, and the winding coils were 1,190 turns of 0.05-mm-diameter wire (internal resistance of 6.5 Ω). The time variations of the internal magnetic flux density caused by periodic bending deformation generate a voltage on the coils according to Faraday's law of induction. The harvester was connected in series to the resistance, R = 10 Ω. The generated voltage V was measured by an A/D converter with a sampling frequency of 2 kHz, and 10^4 data point were stored. The power

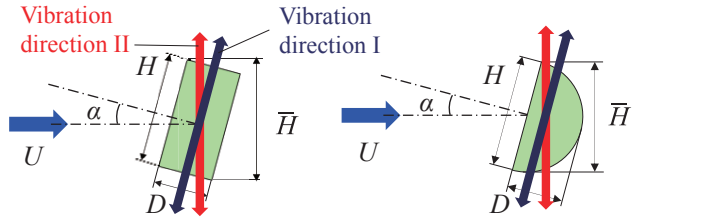

(a) Rectangular prism (b) D-section prism

Figure 1: Cross section of a prism and vibration directions

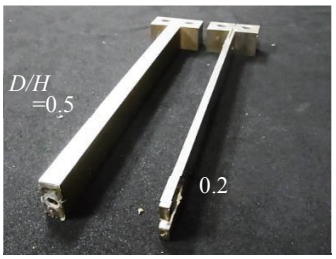

(a) Rectangular prisms

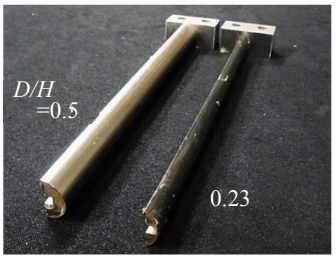

(b) D-section prisms

Figure 3: Test prisms

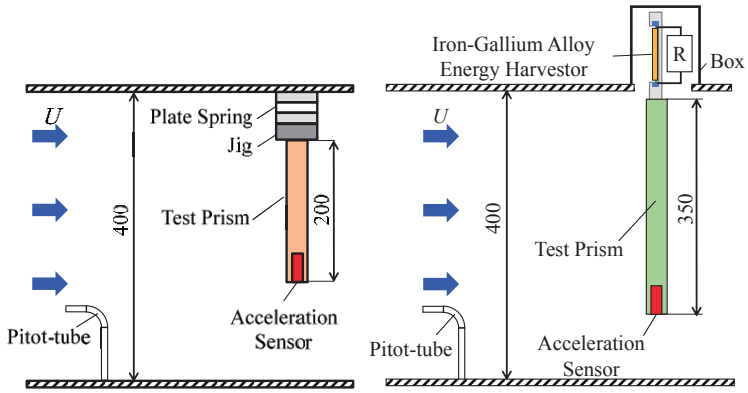

(a) Free-vibration test (b) Power generation test

Figure 2: Schematic diagram of the test section in water tunnel

Table 1: Specification of the test prisms

(a) Free-vibration test

Retangular prism (α=0°)			
D/H	δ	m [kg/m]	Cn
0.5	0.026	1.58	0.42
0.2	0.036	0.65	0.59
D-section prism (α=0°)			
D/H	δ	m [kg/m]	Cn
0.5	0.018	1.35	0.31
0.23	0.023	0.51	0.36

(b) Power generation test

Retangular prism			
D/H	δ	m [kg/m]	Cn
0.2	0.15	0.67	2.4
D-section prism			
D/H	δ	m [kg/m]	Cn
0.23	0.12	0.52	2.0

Table 2: Natural frequency f_c of test prisms

(a) Free-vibration test

Cross section	Rectangular		D-section		
D/H	0.5	0.2	0.5		0.23
Direction I [Hz]	27.0	43.4	25.2 ($\alpha \leq 25$)	28.9 ($\alpha \geq 35$)	46.1
Direction II [Hz]	22.9	35.6	22.8		39.5

(b) Power generation test

Cross section	Rectangular	D-section
D/H	0.2	0.23
Direction II [Hz]	35.9	35.8

generation P (= V_{rms}^2/R) was calculated by a personal computer, where V_{rms} is the effective value of the generated voltage. The tip displacement of the prism y was also measured using an acceleration sensor simultaneously implanted inside the tip of the prism.

3. EXPERIMENTAL RESULT AND DISCCUSION

3.1 FREE-VIBRATION

(1) Vibration direction I

We investigated the response amplitude for the vibration direction I of the rectangular and D-section prisms. The vibration direction I is the same as the longitudinal direction of the prism (Figure 1).

a) Prism with side ratio *D/H* ≈ 0.2

Figure 4 shows the effect of angle of attack α on variation of the root-mean-square value of the amplitudes η_{rms} (= y_{rms}/H) in vibration direction I for a rectangular prism with a side ratio of D/H = 0.2, and a D-section prism with a side ratio of D/H = 0.23 with the reduced velocity V_r (= Uf_c/H). In the case of a rectangular prism with D/H = 0.2 vibration begins to occur near reduced velocity $V_r \approx 1.5$ lower than the resonant velocity and the amplitudes of a prism increase linearly with an increase in the reduced velocity V_r at angle of attack α = 0°. The rectangular prism until α = 25° vibrates the same as one with α = 0°. For $\alpha \geq 30°$, the reduced velocity of the vibration onset for a rectangular prism increases at V_r = 2.1, and a rectangular prism of α = 35° do not occur the vibration. In the case of a D-section prism with D/H = 0.23 at α = 0°, the vibration also begins to occur near reduced velocity $V_r \approx 1.5$ and the amplitudes of a prism increase linearly with an increase in the reduced velocity V_r as with the rectangular prism with D/H = 0.2. In the range of angle of attack between 10° and 45°, a D-section prism vibrates the same as one with α = 0°. The reduced velocity of the vibration onset for a D-section prism of α = 55° increases at V_r = 2.1, and a D-section prism of α = 60° do not occur the vibration. Thus, a D-section prism with D/H = 0.23 can vibrate at the larger angle of attack than a rectangular prism with D/H = 0.2.

Figure 5 shows the response amplitude η_{rms} (= y_{rms}/H) for a rectangular prism and D-section prism with the reduced velocity $\bar{V}_r$ (= $Uf_c/\bar{H}$), which is non-dimensionalized by a characteristics length normal to the incident flow $\bar{H}$, for various angles of attack α. For a rectangular prism with D/H = 0.2, there are a little difference between Figures 4(a) and 5(a). For the D-section prism with D/H = 0.23, as shown in Figure 5(b), the reduced velocity $\bar{V}_r$ of onset of vibration increases as angle of attack α increase. Because $\bar{H}$ decreases as the angle of attack α increase.

b) Prism with side ratio *D/H* = 0.5

Figure 6 shows the effect of angle of attack α on the response amplitudes η_{rms} for a rectangular prism and a D-section prism with side ratio D/H = 0.5 with respect to the reduced velocity V_r in the vibration direction I. In the case of a rectangular prism with D/H = 0.5, a prism at α = 0° begin to vibrate near $V_r \approx 3.0$. The reduced velocity of the vibration onset for a rectangular prism of α = 15° increases at $V_r \approx 3.5$, and the vibration is suppressed gradually at $\alpha \geq 10°$. Especially, the rectangular prism at only α = 20° for V_r = 3.0 − 4.2 vibrates with a half of natural frequency $f_c/2$, i.e. 14 − 17 Hz. This phenomenon has a concern in the change of flow separation point from the leading to trailing edge on the rectangular prism with D/H=0.5 at $\alpha \approx 23°$ [30]. In the case of a D-section prism with D/H = 0.5 at α = 0°, a prism begins to vibrate smaller the reduced velocity at $V_r \approx 2.5$ than a rectangular prism with side ratio D/H = 0.5, and the response amplitude of a D-section prism vibrates until α = 25° the same as α = 0°. The vibration is suppressed at α = 35° and the response amplitudes do not increases more than η_{rms} = 0.02. Thus, a D-section prism with side ratio D/H = 0.5 can vibrate at larger angle of attack than a rectangular prism with side ratio D/H = 0.5.

c) 5 % non-dimensional and increment rate of response amplitude

Figures 7 shows the reduced velocity at the 5 % non-dimensional response amplitude of the prism $V_{r0.05}$ with respect to the angle of attack α. The reduced velocity $V_{r0.05}$ of a rectangular prism with D/H = 0.2 and a D-section prism with D/H = 0.23 is smaller than prisms with D/H = 0.5. The vibration of a D-section prism with D/H = 0.23 is kept until α = 45°. Figures 7 shows the increment rate of the response amplitude for a prism

$d\eta_{rms}/dV_r$, which is the average rate of measured points, with respect to the angle of attack α. The increment rate of the response amplitude $d\eta_{rms}/dV_r$ of a D-section prism with D/H=0.23 are larger than that of a rectangular prism with D/H = 0.2 and a D-section with D/H=0.5. In particular, the increment rate of a D-section prism with D/H=0.23 indicates large value in a wide range of angle of attack until α = 45°.

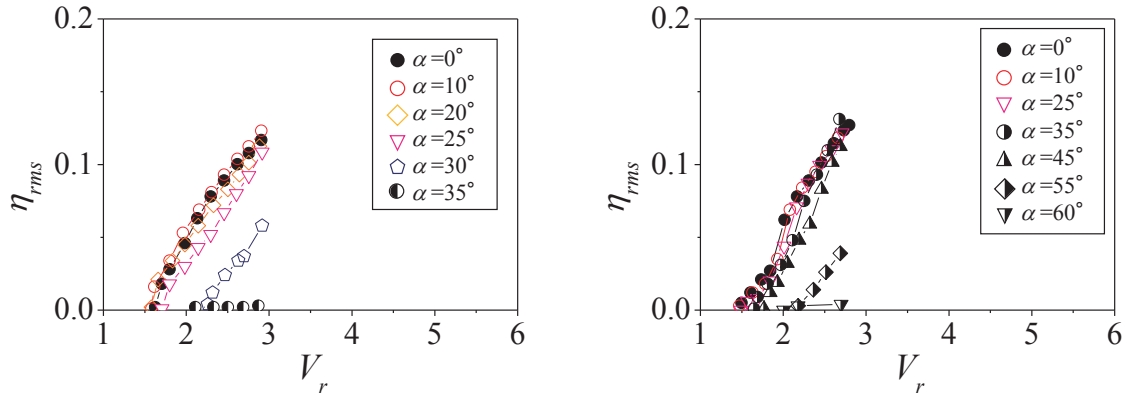

(a) Rectangular prism with D/H=0.2 (b) D-section prism with D/H=0.23

Figure 4: Response amplitude η_{rms} of prism for vibration direction I with respect to the reduced velocity V_r.

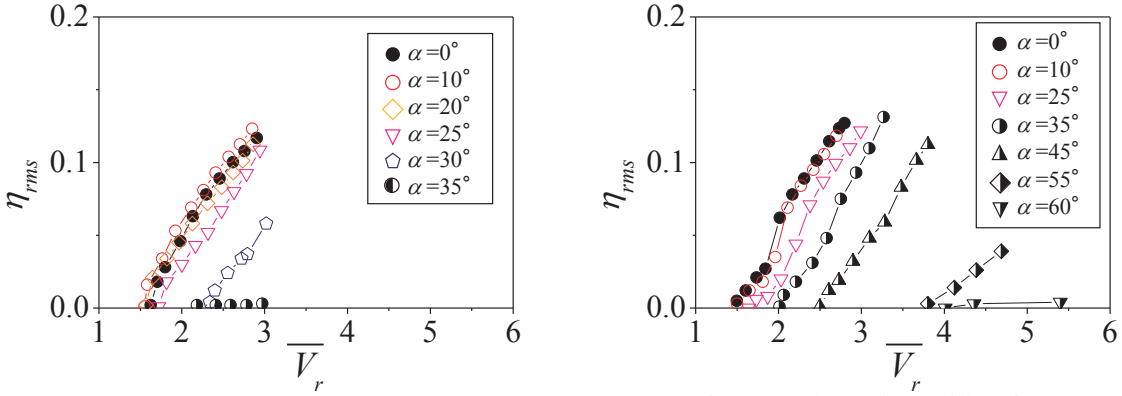

(a) Rectangular prism with D/H=0.2 (b) D-section prism with D/H=0.23

Figure 5: Response amplitude η_{rms} of prism for vibration direction I with respect to the reduced velocity $\overline{V}_r$.

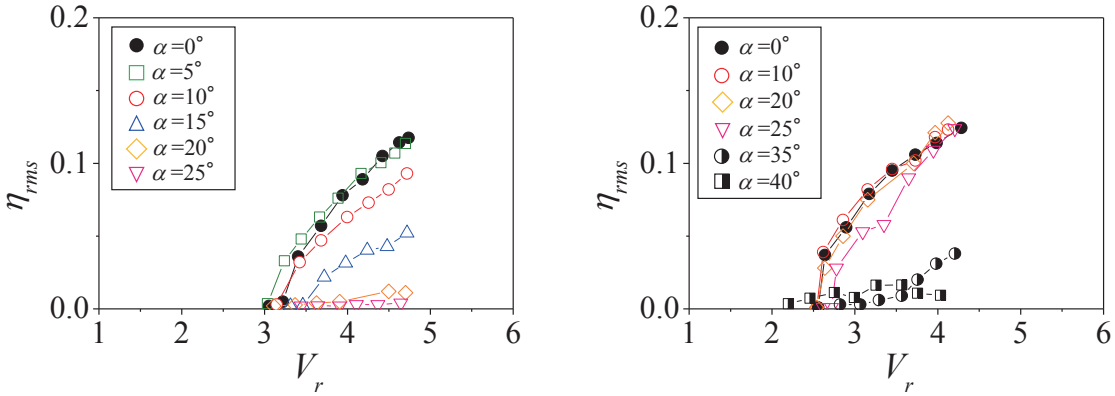

(a) Rectangular prism with D/H=0.5 (b) D-section prism with D/H=0.5

Figure 6: Response amplitude of the prism η_{rms} respect to the reduced velocity V_r with D/H=0.5

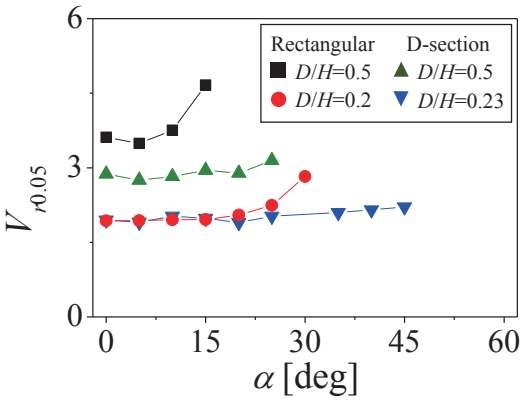

Figure 7: Reduced velocity at the 5% non-dimensional response amplitude $V_{r0.05}$ for direction I

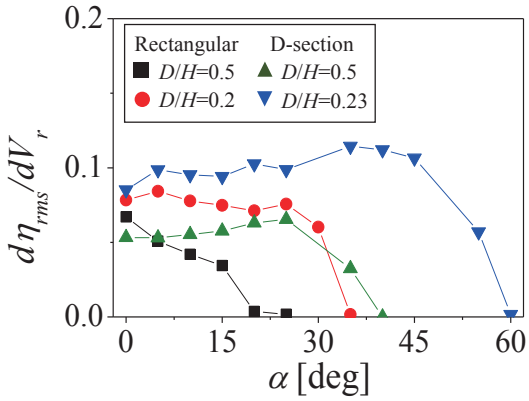

Figure 8: Increment rate of the response amplitude $d\eta_{rms}/dV_r$ for direction I

Knisely presented the Strouhal number for rectangular prisms with side ratios ranging from 0.04 to 1 and with angles of attack from 0° to 90° [30]. For the side ratio of D/H = 0.2, the reattachment of the separated shear layer occurs near 35°. For the side ratio of D/H = 0.5, the reattachment occurs near 20°. Takizawa et al. shows that the lift force of a D-section prism with D/H = 0.5 changes at $\alpha \approx 40°$ [34]. These angles of attack coincide with a change in the response amplitude of prisms. Therefore, the rectangular prism with a small afterbody and D-section prism can vibrate until larger angle of attack.

(2) Vibration direction II

Next, we investigated the response amplitude of the prisms for the vibration direction II, which is the same as the normal direction to flow (Figure 1).

a) Prism with side ratio *D/H* ≈ 0.2

Figure 9 shows the response amplitudes $\overline{\eta}_{rms}$ (=$y_{rms}/\bar{H}$) of a rectangular prism with side ration D/H = 0.2 and a D-section prism with side ration D/H = 0.23 for vibration direction II with respect to the reduced velocity V_r (= Uf_c/H). The response amplitudes of a rectangular prism with D/H = 0.2 increase linearly with an increase in the reduced velocity V_r at angle of attack $\alpha \leq 15°$. The rectangular prism at $\alpha \geq 20°$ vibrates very little. Thus, the range of angle of attack ($0° \leq \alpha < 20°$) in which a rectangular prism with D/H = 0.2 can vibrate for the direction II is narrower than that ($0° \leq \alpha < 35°$) for the direction I. Although a D-section prism with D/H=0.23 for the direction I vibrates at large angle of attack, i.e. α = 45°, the D-section prism for the direction II at α = 15° vibrates very little.

b) Prism with side ratio *D/H* = 0.5

Figure 10 shows the response amplitudes $\overline{\eta}_{rms}$ (=$y_{rms}/\bar{H}$) of the rectangular and D-section prisms with side ration D/H=0.5 for the vibration direction II with respect to the reduced velocity V_r (= Uf_c/H). The response amplitudes of a rectangular prism with D/H = 0.5 increase linearly with an increase in the reduced velocity V_r at angle of attack $\alpha \leq 15°$. The rectangular prism at α = 20° and 25° vibrates slightly. Especially, the rectangular prism at only α = 25° for V_r = 2.5 − 5.2 vibrates with a half of natural frequency $f_c/2$, i.e. 10 − 17 Hz. This phenomenon has a concern in the unsteady flow separation point similar to the rectangular prism with D/H = 0.5 for the vibration direction I. In the case of D-section prism with D/H=0.5, the reduced velocity of the vibration onset increase gradually from V_r = 2.8 of α = 10° to V_r = 3.0 of α = 25°, and the vibration is suppressed at $\alpha \approx 35°$ the same as the vibration direction I.

c) 5 % non-dimensional and increment rate of response amplitude

Figures 11 shows the reduced velocity at the 5 % non-dimensional response amplitude of the prism $V_{r0.05}$ with respect to the angle of attack α. The reduced velocity $V_{r0.05}$ of a rectangular prism with D/H = 0.2 and a D-section prism with D/H=0.23 is smaller than prisms with D/H=0.5. The vibration of a D-section prism with D/H=0.5 is kept until α = 25°. Figures 7 shows the increment rate of the response amplitude for a prism d $\overline{\eta}_{rms}$

/dV_r with respect to the angle of attack α. Although the increment rate of the response amplitude d$\overline{\eta}_{rms}$/dV_r of a D-section prism with D/H=0.23 are larger, the range of vibratile angle of attack is narrower than the other prism. In particular, the increment rate of the response amplitude d$\overline{\eta}_{rms}$/dV_r of a D-section prism with D/H=0.5 indicates large value in a wide range of angle of attack until α = 30°.

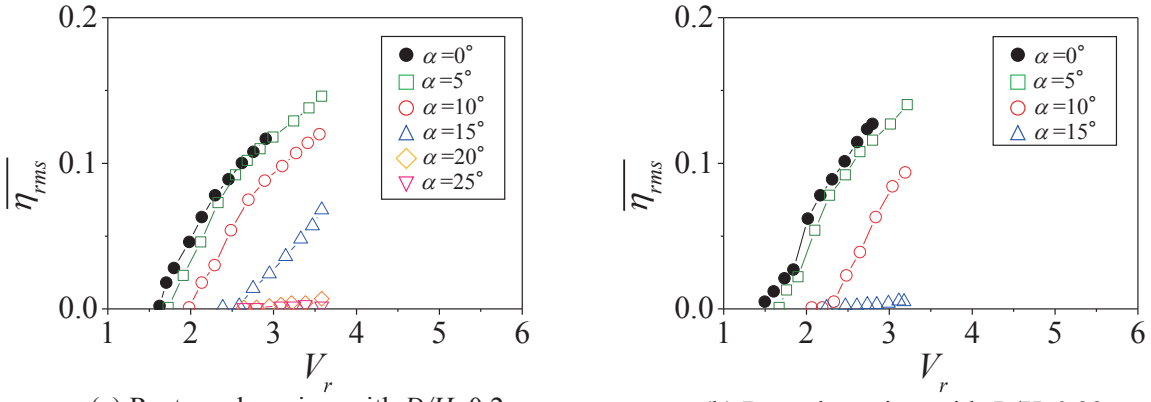

(a) Rectangular prism with D/H=0.2

(b) D-section prism with D/H=0.23

Figure 9: Response amplitude of the prism $\overline{\eta_{rms}}$ respect to the reduced velocity V_r with D/H≈0.2

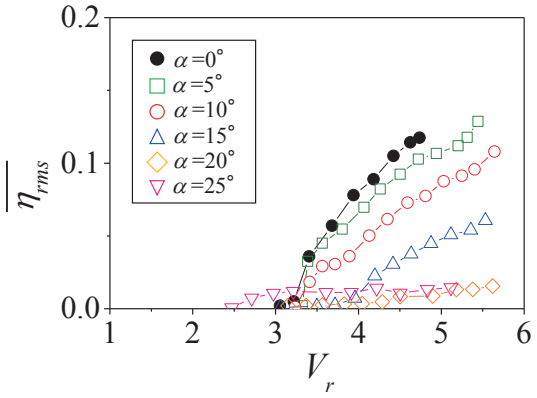

(a) Rectangular prism with D/H=0.5

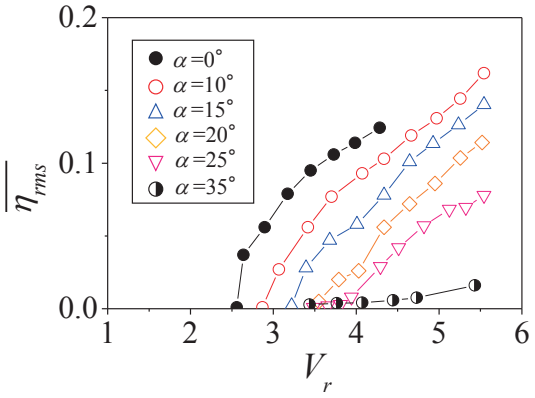

(b) D-section prism with D/H=0.5

Figure 10: Response amplitude of the prism $\overline{\eta_{rms}}$respect to the reduced velocity V_r with D/H=0.5

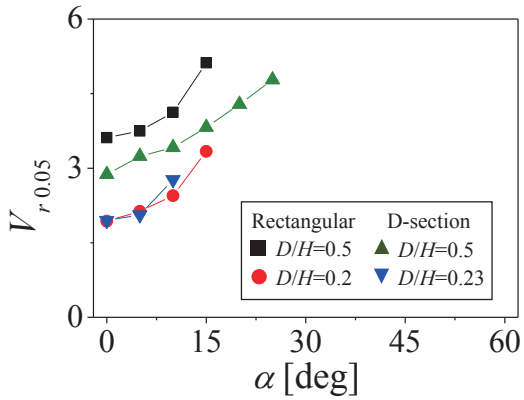

Figure 11: Reduced velocity at the 5% non-dimensional response amplitude $V_{r0.05}$ for direction II

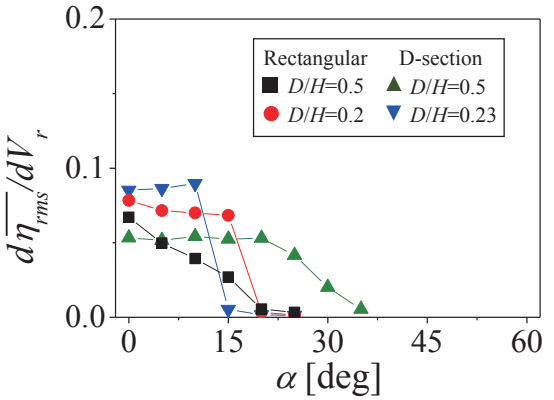

Figure 12: Increment rate of the response amplitude d$\overline{\eta_{rms}}$/dV_r for direction II

3.2 VIBRATION-POWER GENERATION

From the result of free-vibration experiment, the prisms with small side ratio for the vibration direction I are suitable for the power generation of flow-induced vibration. So, the power generation experiment is conducted by using a rectangular prisms with side ratio D/H = 0.2 and a D-section prisms with side ratio D/H = 0.23. Figures 13 and 14 show time histories of the response amplitudes and the generated voltage at α = 0° and 25°. Although there is a phase difference between waveforms of amplitude and voltage, each waveform of the amplitudes and voltages is almost stable against times. Figure 15 shows the response amplitudes η_{rms} (= y_{rms}/H) and the generated power P of a rectangular prisms with side ratio D/H = 0.2 and a D-section prisms with side ratio D/H = 0.23 at angles of attack α = 0° and 25°. The response amplitudes and the generated power increase with increase of the reduced velocity. There are no marked difference between α = 0° and α = 25° on the response amplitudes and generated power. The generated power at Vr = 4.15 for a D-section prism is about 26 mW. Figure 16 shows the coefficient of power generation of the prisms with respect to the reduced velocity.

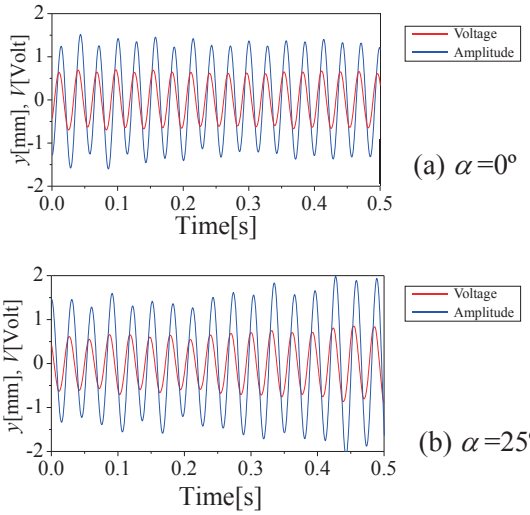

Figure 13: Time history of the response amplitudes of rectangular prism and generated voltage at V_r=3.6

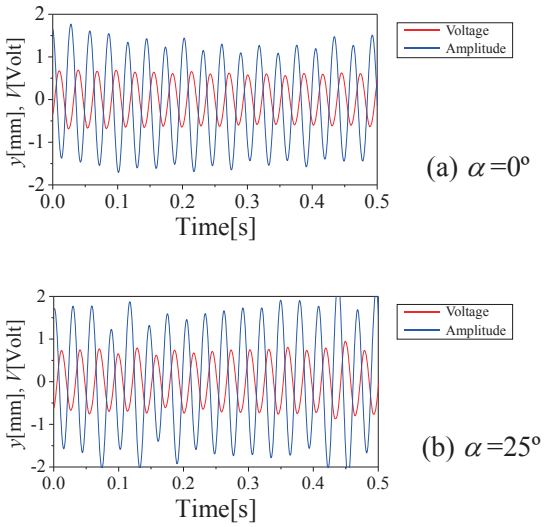

Figure 14: Time history of the response amplitudes of D-section prism and generated voltage at V_r=3.8

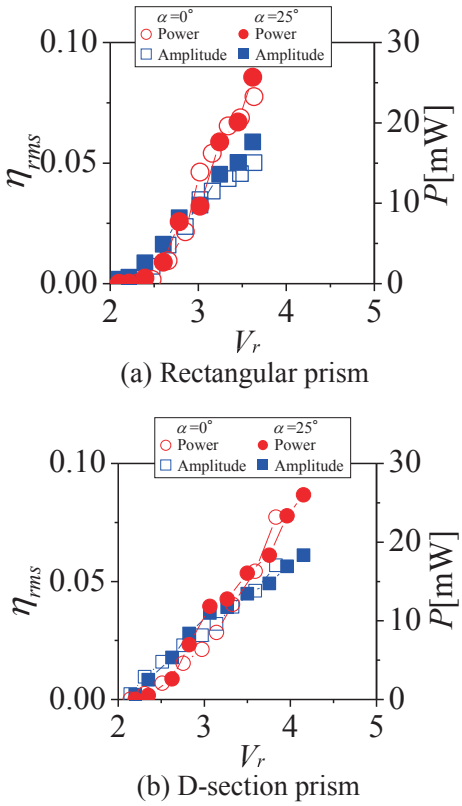

Figure 15: Response amplitudes of a prism and generated power

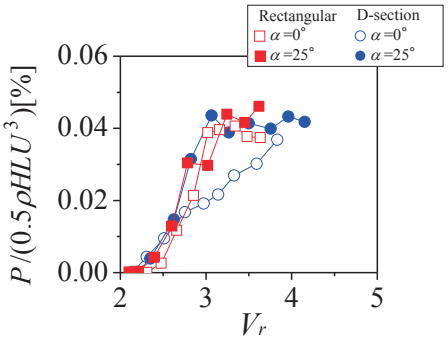

Figure 16: Coefficient of power generation

For $V_r > 3$, the coefficient of power generation becomes saturated. Maximum coefficient of power generation of the prism is about 0.045%.

4. CONCLUSIONS

Free-vibration and power generation tests using rectangular and D-section prisms with side ratio $D/H \approx 0.2$ and 0.5 were performed in a water tunnel. The main conclusions of the present study are as follows:

(1) For the vibration direction I which is the same as the longitudinal direction of the prism, the D-section prism with side ratio $D/H = 0.23$ has the highest increment rate of the response amplitude, and vibrates in the wide range of angle of attack than the other prisms.

(2) For the vibration direction II which is the normal direction to flow, the D-section prism with side ratio $D/H = 0.23$ has the highest increment rate of the response amplitude. The range of vibratile angle of attack is narrower than that for the vibration direction I.

(3) The generated power and the maximum coefficient of the prism for the vibration direction I are 26 mW and 0.045 %, respectively.

ACKNOWLEDGMENT

The authors are thankful to Dr. Okajima for productive discussions and to technician Mr. Kuratani for his help with the experiment.

REFERANCES

1) Sodano,H.A., Inman,D.J. and Park,G., "A Review of Power Harvesting from Vibration using Piezoelectric Materials," *Smart Materials and Structures*, Vol.16, No.3, pp.1-9, 2007.
2) Uno,M. and Kawashima,R., "Proposal of Oscillating Type Hydraulic Power Generation, " *Proceedings of Renewable Energy 2010*, Yokohama, Japan, Paper No.P-Sh-7, pp.1–4, 2010.
3) Hiejima,S., Oka,K., Hayashi,K. and Inoue,H., , "Investigation on Energy Harvesting Efficiency for Flow-induces Vibration Based Power Generation Using Inverted Pendulum," *Proceedings of the 22nd National Symposium on Wind Engineering*, Tokyo, Japan, pp.425–430, 2012 (in Japanese).
4) Tanaka,Y., Matsumura,K. and Mutsuda,H., "Study on Flexible Power Generation Device Using Piezoelectric Film," *Journal of Energy and Power Engineering*, Vol.6, pp.353–360, 2012.
5) Fei,F., Mai,J.D. and Li,W.J., "A Wind-flutter Energy Converter for Powering Wireless Sensors," *Sensors and Actuators A*, Vol.173, pp.163–171, 2012.
6) Kwon,S.D., Lee,H. and Lee,S., "Wind Energy Harvesting from Flutter," *Proceedings of the 13th International Conference on Wind Engineering*, Amsterdam, Netherlands, 071_8page, pp.1-5, 2011.
7) Ali,M., Arafa,M. and Elaraby,M., "Harvesting Energy from Galloping Oscillations," *Proceedings of the World Congress on Engineering 2013*, London, U.K., Vol. III, pp.1–6, 2013.
8) Qiang Zhu, Max Hasse and Chin H. Wu, "Modeling the capacity of a novel flow-energy harvester", Applied Mathematic Modelling, Vol.33 No.5, pp.2207-2217, 2009.
9) Parkinson,G.V. and Smith,J.D., "The Square Prism as Aeroelastic Non-Linear Oscillator," *The Quarterly Journal of Mechanics and Applied Mathematics*, Vol. 17, pp.225–239, 1964.
10) Van Oudheusden,B.W., "On the Quasi-steady Analysis of One-degree-of-freedom Galloping with Combined Translational and Rotational Effects," *Nonlinear Dynamics*, Vol.8, pp.435–451, 1995.
11) Luo,C., Chew,Y.T. and Ng,Y.T., "Hysteresis Phenomenon in the Galloping Oscillation of a Square Cylinder.", *Journal of Fluids and Structures*, Vol.18, pp.103–118, 2003.
12) Tamura,T. and Dias,P.P.N.L., "Unstable Aerodynamic Phenomena Around the Resonant Velocity of a Rectangular Cylinder with Small Side Ratio," *Journal of Wind Engineering and Industrial Aerodynamics*, Vol.91, pp.127-138, 2003.
13) Nakamura, Y., Hirata,K. and Urabe,T., "Galloping of rectangular cylinders in the presence of a splitter plate," *Journal of Fluids and Structures*, Vol.5, pp. 521-549, 1991.
14) Kiwata,T., Yamaguchi,M., Kono,T. and Ueno,T., "Water tunnel experiments on transverse-galloping of

cantilevered rectangular and D-section prisms," *Journal of Fluid Science and Technology,* Vol. 9, No. 3, http://doi.org/10.1299/jfst.2014jfst0056, pp.1-11, 2014.
15) Kiwata,T., Yamaguchi,M., Nakajima,A., Kono,T. and Ueno,T., "Flow-Induced Transverse Vibration of a Cantilevered Prism for Energy Harvesting", *Proceedings of the ASME 2014 Pressure Vessels & Piping Division Conference*, California, USA, PVP2014-28939, pp.1-10, 2014.
16) Bokaian,A.R. and Geoola,F., "On the Cross Flow Response of Cylindrical Stryctures", *Proceedings Institution Civil Engineers*, London, Vol.75, Paper8654, pp.397-418, 1983.
17) Alonso,G. and Meseguer,J., "A Parametric Study of the Galloping Stability of Two-dimensional Triangular Cross-section Bodies," *Journal of Wind Engineering and Industrial Aerodynamics*, Vol. 94, pp.241–253, 2006.
18) Luo,S.C., Yazdani,M.G., Chew,Y.T. and Lee,T.S., "Effects of Incidence and Afterbody Shape on Flow Past Bluff Cylinders," *Journal of Wind Engineering and Industrial Aerodynamics*, Vol.53, pp.375–399, 1993.
19) Luo,S.C., Chew,Y.T. and Yazdani,M.G., "Stability to Translational Galloping Vibration of Cylinders at Different Mean Angles of Attack", *Journal of Sound and Vibration*, Vol.215, pp.1183–1194, 1998.
20) Barrero-Gil,A., "Energy Harvesting from Transverse Galloping," *Journal of Sound and Vibration*, Vol.329, pp.2873–2883, , 2010.
21) Kluger, J.M., Moon, F.C. and Rand,R.H., "Shape Optimization of a Blunt Body Vibro-wind Galloping Oscillator," *Journal of Fluids and Structures*, Vol. 40, pp.185-200, 2013.
22) Naudascher,E. and Rockwell,D., "Flow-induced Vibrations: An Engineering Guide," Dover Publications, Inc., 2005.
23) Ueno,T. and Yamada,S., "Performance of Energy harvester using Iron-Gallium Alloy in Free Vibration," *IEEE Transactions on Magnetics*, Vol.47, pp. 2407–2409, 2010.
24) Japan Society of Mechanical Engineers, "Guideline for Evaluation of Flow-induced Vibration of a Cylindrical Structure in a Pipe," JSME S 012-1998, pp.B6-B14, Maruzen Co. Ltd., 1998 (in Japanese).
25) Nakaguchi,H., Hashimoto,K. and Muto,S., "An Experimental Study on Aerodynamic Drag of Rectangular Cylinders," *Journal of Japan Society for Aeronautical and Space Sciences*, Vol. 16, No. 168, pp.1-5 , 1968 (in Japanese).
26) Okajima,A., Kimura,S., Katayama,T., Ohtsuyama,S. and Ojima,A., "Fluid-dynamic Characteristics of a Rectangular Cylinder with Various Width-to-ratios in Wide Range of Reynolds Number," *Journal of Structural Engineering*, Vol.44A, pp.971-977, 1998 (in Japanese).
27) Ohya,Y., "Note on a Discontinuous Change in Wake Pattern for a Rectangular Cylinder", *Journal of Fluids and Structures*, Vol.8, pp.325-330, 1994.
28) Feng,C.C., 1968, "The Measurement of Vortex Induced Effects in Flow Past Stationary Circular and D-section Cylinder," *Thesis of M.A.Sc., The University of British Columbia*.
29) Tamura,T. and Miyagi,T., "The effect of turbulence on aerodynamics force on a square cylinder with various corner shapes", *Journal of Wind Engineering*, Vol.83, pp.135-145, 1999.
30) Knisely,C.W., "Strouhal numbers of rectangular cylinders at incidence: A review and new data", *Journal of Fluids and Structures*, Vol.4, No.4, pp.371-393, 1990
31) Alonso,G., Valero,E. and Meseguer,J., "An analysis on the dependence on cross section geometry of galloping stability of two-dimensional bodies having either biconvex or rhomboidal cross sections", *European Journal of Mechanics B/Fluids*, Vol.28, No.2, pp.328-334, 2009
32) Matsumoto,M., Ishizaki,H., Matsuoka,C., Daito,Y., Ishikawa,Y. and Shimahara,A., "Aerodynamic effects of the angle of attack on a rectangular prism", *Journal of Wind Engineering and Industrial Aerodynamics*, Vol.77-78, pp.531-542, 1998
33) Naudascher,E. and Wang,Y., "Flow-Induced Vibrations of Prismatic Bodies and Grids of Prisms", *Journal of Fluids and Structures*, Vol.7, No.4, pp.341-343, 1993.
34) Takizawa,N., Okada,N., Iwasaki,A., "Wind-tunnel Investigation of Pressure Distribution and Deduced Characteristics of Semi-Circular Cylinder in the Vicinity of Critical Reynolds Number," Technical Report of National Aerospace Laboratory, TR-871, pp.1-42, 1985 (in Japanese).